Title

Biological substrate modification suppresses ventricular arrhythmias in a porcine model of chronic ischaemic cardiomyopathy.

Journal

European Heart Journal, 43(22)

ISSN

0195-668X

Authors

Dawkins, James F
Ehdaie, Ashkan
Rogers, Russell
et al.

Publication Date

2022-06-06

DOI

10.1093/eurheartj/ehac042

Peer reviewed

ESC European Society of Cardiology

European Heart Journal (2022) **43**, 2139–2156
https://doi.org/10.1093/eurheartj/ehac042

TRANSLATIONAL RESEARCH
Arrhythmias

Biological substrate modification suppresses ventricular arrhythmias in a porcine model of chronic ischaemic cardiomyopathy

James F. Dawkins [1], Ashkan Ehdaie [1], Russell Rogers [1], Daniel Soetkamp[1], Jackelyn Valle[1], Kevin Holm[1], Lizbeth Sanchez[1], Ileana Tremmel [1], Asma Nawaz[1], Michael Shehata[1], Xunzhang Wang[1], Adityo Prakosa [2], Joseph Yu [2], Jennifer E. Van Eyk[1], Natalia Trayanova[2], Eduardo Marbán [1], and Eugenio Cingolani[1]*

[1]Smidt Heart Institute, Cedars-Sinai Medical Center, 8700 Beverly Blvd, Los Angeles, CA 90048, USA; and [2]Alliance for Cardiovascular Diagnostic and Treatment Innovation, Department of Biomedical Engineering, Johns Hopkins University, Baltimore, MD, USA

Received 14 May 2021; revised 25 January 2022; accepted 26 January 2022; online publish-ahead-of-print 9 March 2022

See the editorial comment for this article 'A novel exosome-based therapy for post-MI arrhythmias', by Marine Cacheux and Fadi G. Akar, https://doi.org/10.1093/eurheartj/ehac155.

Aims Cardiomyopathy patients are prone to ventricular arrhythmias (VA) and sudden cardiac death. Current therapies to prevent VA include radiofrequency ablation to destroy slowly conducting pathways of viable myocardium which support re-entry. Here, we tested the reverse concept, namely that boosting local tissue viability in zones of slow conduction might eliminate slow conduction and suppress VA in ischaemic cardiomyopathy.

Methods and results Exosomes are extracellular vesicles laden with bioactive cargo. Exosomes secreted by cardiosphere-derived cells (CDC_{EXO}) reduce scar and improve heart function after intramyocardial delivery. In a VA-prone porcine model of ischaemic cardiomyopathy, we injected CDC_{EXO} or vehicle into zones of delayed conduction defined by electroanatomic mapping. Up to 1-month post-injection, CDC_{EXO}, but not the vehicle, decreased myocardial scar, suppressed slowly conducting electrical pathways, and inhibited VA induction by programmed electrical stimulation. *In silico* reconstruction of electrical activity based on magnetic resonance images accurately reproduced the suppression of VA inducibility by CDC_{EXO}. Strong anti-fibrotic effects of CDC_{EXO}, evident histologically and by proteomic analysis from pig hearts, were confirmed in a co-culture assay of cardiomyocytes and fibroblasts.

Conclusion Biological substrate modification by exosome injection may be worth developing as a non-destructive alternative to conventional ablation for the prevention of recurrent ventricular tachyarrhythmias.

* Corresponding author. Email: eugenio.cingolani@csmc.edu

Key question

Can biologic therapy provide a non-destructive method to decrease ventricular tachycardia (VT) in ischaemic cardiomyopathy?

Key finding

Injection of exosomes secreted by cardiosphere-derived cells (CDC_{EXO}) reduced inducible arrhythmias and cardiac scar while improving left ventricular function.

Take-home message

Focal delivery of CDC_{EXO} in areas of late activation represents a novel, non-destructive substrate modification strategy to prevent VT.

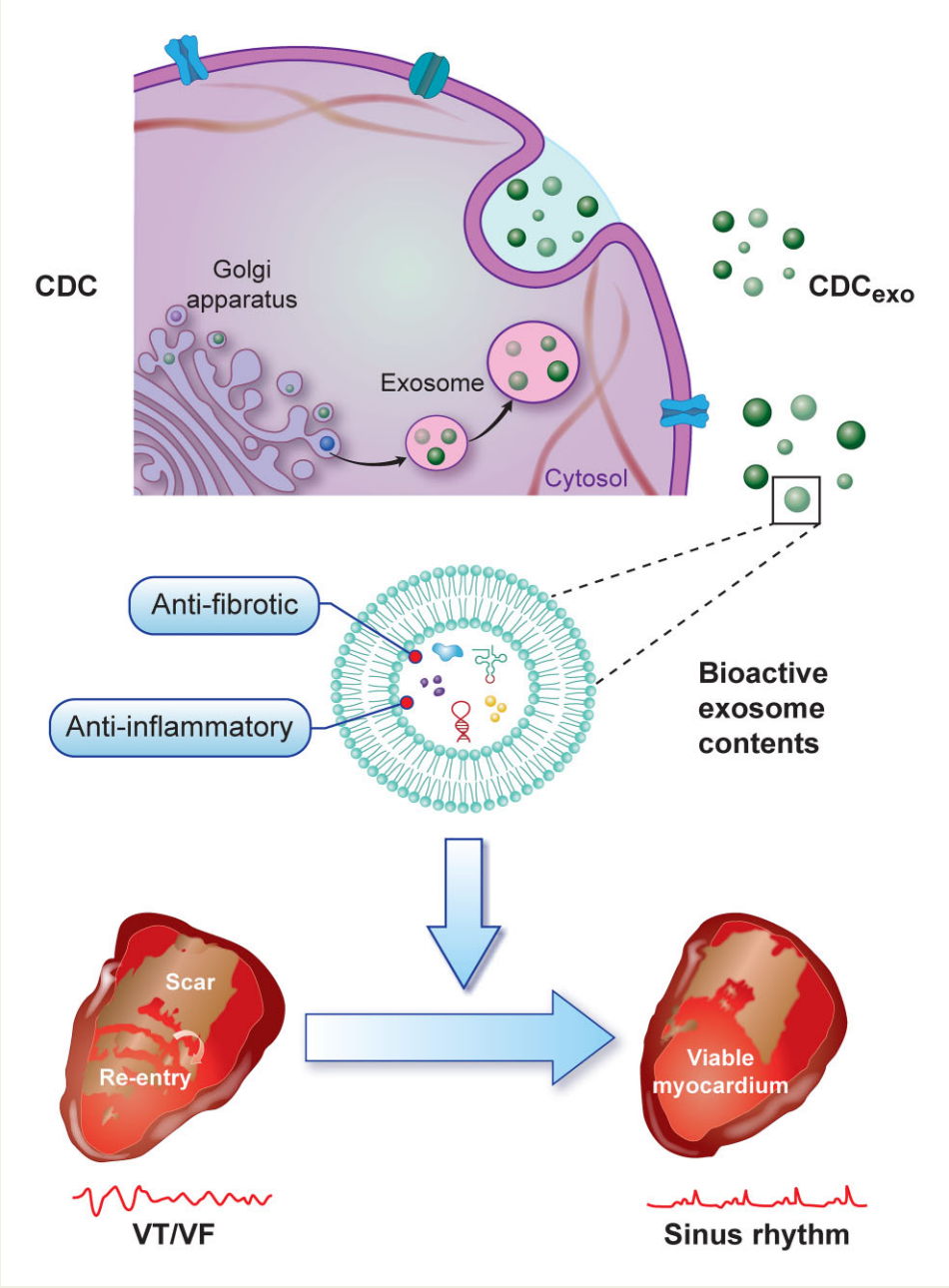

Structured Graphical Abstract Salutary effects of intramyocardial delivery of exosomes secreted by cardiosphere-derived cells (CDC_{EXO}) in ischaemic cardiomyopathy.

Keywords Arrhythmia • Ventricular tachycardia • Cardiac stem cells • Cardiosphere-derived cells • Exosomes • Heart failure • Myocardial infarction • Ischaemic cardiomyopathy

Translational perspective

Ventricular tachyarrhythmias often underlie haemodynamic collapse and sudden death. While ablation can suppress recurrent ventricular tachyarrhythmias, efficacy is limited and major complications, including exacerbation of heart failure, occur frequently in cardiomyopathy patients. Here, we explored a complementary strategy: rather than destroying heart tissue, we sought to modify the substrate using anti-fibrotic exosomes secreted by cardiosphere-derived cells (CDC_{EXO}). In pigs with ischaemic cardiomyopathy, we injected CDC_{EXO} into zones of delayed conduction. Two to four weeks later, the ability to induce ventricular arrhythmias (VA) was markedly suppressed. Biological substrate modification may be a viable, non-destructive alternative to ablation to suppress VA.

Introduction

Cardiomyopathies, which underlie the global heart failure epidemic, predispose to ventricular arrhythmias (VA) and sudden cardiac death.[1] Indeed, the finding of low cardiac pump function suffices as an indication for a prophylactic implantable cardioverter-defibrillator (ICD).[2] The presence of an ICD provides a safety net when tachyarrhythmias occur, shocking the heart back into sinus rhythm. However, many cardiomyopathy patients have zones of scar within their hearts mixed with strands of living heart muscle, setting up re-entrant circuits of excitation which precipitate ventricular tachycardia (VT).[3] Patients with ICDs may survive the VT, but, if the substrate favours recurrent re-entry, multiple repeated shocks ensue, leading, in the extreme, to 'electrical storm'.[2] Anti-arrhythmic drugs are inconsistently effective and have major side effects.[4] The only remaining treatment option is targeted destruction ('ablation') of the heart tissue which underlies slow conduction.[5] In heart failure patients with VT, ablations are frequently unsuccessful, and even when initially effective, recurrence rates are high.[5] Moreover, the purposeful destruction of heart tissue, even if targeted, can diminish pump function and exacerbate heart failure. Alternative approaches are clearly desirable.

Rather than destroying slowly conducting tissue, an anti-fibrotic strategy could, in principle, improve conduction and thereby disable re-entry. Cardiosphere-derived cells (CDCs) are therapeutic candidates currently in clinical testing for various forms of cardiovascular disease.[6] Exosomes secreted by CDCs (CDC_{EXO}) are anti-fibrotic: they decrease scar and improve contractile function when injected intramyocardially in models of ischaemic cardiomyopathy.[7] With the primary endpoint being the elimination of sustained inducible arrhythmias and a secondary surrogate endpoint of local reduction of scar, we tested the hypothesis that targeted injection of CDC_{EXO} into zones of slow conduction will prevent the inducibility of VA. To do so, we implemented a porcine model of chronic myocardial infarction (MI), performed magnetic resonance imaging (MRI), and demonstrated the ready inducibility of VT by programmed electrical stimulation (PES). We then pinpointed zones of slow conduction using electroanatomical mapping (EAM) and injected CDC_{EXO} (or vehicle) percutaneously into those areas of the heart.

Materials and methods

Cardiosphere-derived cell exosome isolation

Human CDCs were grown in 45 Nunc TripleFlask-treated cell culture flasks to confluency at fifth passage (from a single non-diseased human donor). Cardiosphere-derived cells were grown until confluence in 20% complete CDC culture media. Cardiosphere-derived cells were washed four times with phosphate-buffered saline (PBS) (to remove any residual fetal bovine serum-derived exosomes) and changed to serum-free media. After 15 days, the conditioned media were collected, filtered through a 450 nm filter, and exosomes isolated by ultrafiltration by centrifugation followed by overnight precipitation in 25% poly-ethylene glycol (PEG). The media containing PEG were centrifuged for 30 min at 2000 *g*, and the exosome pellet (7.5 mg of protein by Bradford assay/16.5×10^{11} particles by NanoSight® for characterization) was resuspended in 2 mL of Iscove's modified Dulbecco's medium (IMDM) for injection.

Swine infarct model

Myocardial infarction was induced in 34 female Yucatan mini-pigs. Age-matched animals of similar size (30–35 kg) were enrolled, facilitating a favourable growth curve over the 2-month experimental protocol. A standard balloon angioplasty catheter (TREK) was advanced distal to the first diagonal branch at the proximal third of the left anterior descending (LAD) artery. The balloon was inflated for 90 min, followed by 8 weeks of reperfusion. Cardiac MRI was performed during Week 8, followed by an electrophysiology study, electroanatomic mapping, and endocardial CDC_{EXO} delivery (see below for details) using a NOGA Myostar® catheter. This study was performed on a protocol approved by the institutional animal care and use committee at Cedars-Sinai Medical Center.

Magnetic resonance imaging

Magnetic resonance imaging was performed on a 3.0 T MRI scanner (Siemens, Germany) 8 weeks following MI, and 2 weeks (or 1 month, as indicated) following the delivery of CDC_{EXO}. The scar size [scar mass divided by left ventricular (LV) mass], LV chamber volumes, and LV ejection fraction (LVEF) were measured using image processing software (Circle Cardiovascular Imaging Inc., Canada). Six-millimetre short-axis slices were acquired from the apex to the mitral valve plane. Left ventricular volumes were assessed using electrocardiographic (ECG)-gated, breath-hold, cine steady-state free precession acquisitions. The scar mass and scar size were calculated using delayed contrast-enhanced sequences (acquired 8 min following intravenous injection of gadolinium-based contrast agent). The scar area was defined by hyper-enhanced myocardium using mean 5× the standard deviation of healthy myocardium.

Electrophysiology study

A quadripolar catheter connected to an electronic recording/stimulator system (St Jude Medical) was used for PES at baseline

and study endpoint. The catheter was advanced under fluoroscopic guidance and first positioned at the LV border zone (BZ), and then the right ventricular (RV) apex. A drive train of eight beats (S1 at 400 ms), at 20 mA and a pulse width of 2 ms followed by up to three extra stimuli (S2–S4) with progressively decreasing cycle length (−10 ms) until the effective refractory period was reached at each location.

Electroanatomical mapping and exosome delivery

High-density activation and voltage mapping were performed using Rhythmia system (Boston Scientific). Intracardiac electrograms were acquired with the Orion mini-basket catheter, deploying a 64-electrode array on a mini-basket, and advanced through a carotid artery sheath, past the aortic valve to the LV apex. Local activation was determined during sinus rhythm based on bipolar electrograms and unipolar electrogram morphology and catheter contact with reproducible near-field potentials. Data acquisition was automated utilizing established acceptance criteria: total cycle length stability (±5 ms), 12-lead ECG morphology match, time stability of a reference electrogram positioned at the RV apex, and beat-to-beat ECG consistency (≥3 beats with similar electrogram morphology and timing and respiratory stability). Electrograms were classified as either normal or having late multicomponent deflections according to standard criteria.[8] Normal electrograms from porcine species have three or fewer sharp intrinsic deflections from baseline, amplitude ≥3 mV, duration <65 ms. Isolated late potentials were identified with a near-field amplitude >0.3 mV and identified by displaying an additional signal separated from the local ventricular electrogram by >20 ms following the isoelectric interval, while meeting general beat acceptance criteria described above. Late potentials were quantified manually from high-density maps by two independent blinded reviewers.

Eight weeks post-MI, animals were randomized to receive intramuscular injection of vehicle (IMDM) or CDC_{EXO} (7.5 mg protein). Low-density EAM was performed using NOGA® EAM system followed by injection through a Myostar® catheter. The location of previously identified bipolar ORION catheter tip potentials served as a fluoroscopic reference for the NOGA map. Animals were then followed for 2 weeks or 1 month, when high-density EAM, MRI, and PES were repeated prior to sacrifice. Bipolar map potentials from the Myostar® catheter confirmed previously identified late potentials. Once identified, 9–10 injections were performed in those regions where late potentials were recorded.

Conduction velocity measurements

To determine conduction velocity (CV), Rhythmia mapping data were exported into MATLAB (MathWorks) format and analysed by custom software using discrete electrode position (*x*, *y*, and *z*) in space relative to a reference electrode, and the bipolar time of each electrode readings in milliseconds. Because each sample contained different patterns of data point sampling and varying proportions of healthy, borderline, and scar tissue, sections of each heart sample were analysed to determine the optimal portion to sample for CV calculations. To do this, each sample was sliced into 10 (arbitrary number) sections of equal width, with the plane of each slice perpendicular to the propagation of depolarization. Activation maps were generated showing overall bipolar voltage readings (mV) at each electrode point. Once the slices were defined, the data point density of each slice was arranged in descending order, and the top three densest slices were isolated for further examination. The voltage readings of the points in each of the three densest slices were then averaged, and the slice with the lowest voltage reading was chosen as the final region of interest, given that low voltage indicates dense scar. The instantaneous velocities of all points in that region were then calculated and averaged to get the final CV, by calculating the Euclidean distance between consecutive pairs of points in the region and dividing that distance by the difference in time readings between those points. Instantaneous velocities were averaged to derive final CV.

Histology

Samples from the infarcted zone (IZ), BZ, and remote zone (RZ) were cut into 4 μm sections after fixation in 10% formalin and paraffin embedding. Slides were then deparaffinized and stained with Picrosirius red for evaluation of collagen deposition. A subset of eight animals was selected for the evaluation of cell proliferation by Ki67, AKB, and PHH3. Following deparaffinization, immunohistochemistry was visualized by confocal microscopy at 63×. Slides were stained with alpha-sarcomeric actinin (α-SA), wheat germ agglutination (WGA), and 4′,6-diamidino-2-phenylindole (DAPI). See Supplementary *Table S2* for details. Haematoxylin and eosin staining was then performed in the same subset of animals to evaluate the non-cardiomyocyte population. Image J was used for analysis.

Computational cardiology

A biophysically detailed three-dimensional ventricular model of each porcine heart was constructed from the contrast-enhanced MRI scans. Left ventricular walls were segmented semi-automatically as described.[9,10] Pixels were classified as infarcted, grey zone (GZ), or non-infarcted based on thresholding of signal intensity. Two models of the same porcine heart were constructed, one before and another after CDC_{EXO} injection, reflecting the structural remodeling around injection sites. Fibre orientation was incorporated in the reconstructed model as described.[11] As described,[12] we tested the inducibility of each ventricular model for sustained arrhythmia from different pacing sites, using a validated software platform.[13]

Proteomics

Heart tissue samples from IZ, BZ, and RZ were quickly rinsed in cold isolation buffer [250 mM sucrose, 10 mM HEPES, 2.5 mM EDTA, and 1× protease inhibitor (Roche), pH 7.4], snap frozen in liquid nitrogen, and stored at −80°C until processing for mass spectrometry (MS). Further tissue processing including trypsin digestion and the MS methods were as described.[14] Briefly, the MS data were obtained using data-dependent acquisition using a 60 min gradient on an Orbitrap Elite Hybrid MS (ThermoFisher). Mass spectrometry data were searched against the concatenated target/decoy human and pig Uniprot database and, with only reviewed and canonical sequences used. As the pig annotated protein database is underrepresented, the MS data were searched using against the concatenated target/decoy human and pig Uniprot

database with only reviewed and canonical sequences used to maximize protein identification (compare 20 214 vs. 9823 proteins in the annotated Uniprot databases, respectively). All protein identifications were based on a minimum of two non-overlapping tryptic peptides and isoforms were assigned only if a peptide was observed with an amino acid sequence unique to the isoform. Pairwise comparisons between experimental groups were performed using the *t*-test and protein abundance differences of $P < 0.05$ were considered significantly different. For ingenuity pathway analysis, differentially expressed proteins (DEPs) from each myocardial zone and their corresponding $\log_2$FC values were used to define enriched pathways, and upstream regulators. The following parameters were used for these analyses: (i) human genes in the Ingenuity Knowledge Base were used as the reference set; (ii) both the direct and indirect relationships were considered; and (iii) the confidence level was set to be 'experimentally observed' and 'high predicted' with high confidence score. *P*-values for the identified canonical pathways, disease associations, and functions were calculated using Fisher's exact test. The Benjamin–Hochberg method was used to estimate the false discovery rate (FDR), and an FDR-corrected *P*-value of 0.05 was used to select significantly enriched pathways.

In vitro fibrosis model

Neonatal rat ventricular myocytes (NRVMs) were isolated as described.[15] The cells were plated on fibronectin-coated Nunc Lab-Tek II Chamber slide (Thermo Scientific) at a density 700 000 thousand cells/chamber and cultured as described.[16–18] Primary cardiac fibroblasts were co-cultured at 100 000 thousand cells/chamber. The co-culture of NRVMs with fibroblasts was cultured for 2 weeks. On the day of treatment, 10 ng of recombinant mouse transforming growth factor (TGF)-β1 (carrier-free) (Bio Legend) was added daily for 2 weeks in serum-reduced media for all groups. On Day 5 of TGF-β1 treatment, each culture plate underwent one of the three interventions: addition of vehicle, addition of 2.5 mM pirfenidone (Sigma),[19] or addition of CDC_{EXO} (see below). Five days after treatment, Masson's trichrome and immunocytochemistry were performed on the co-cultures. Exosome preparations were analysed through Malvern Nanosight NS300 instrument (Malvern Instruments) with the following acquisition parameter: camera level of 12, detection level ≤ 5, number of videos taken = 4. On Day 5 of TGF-β1 treatment, a total of 7.0×10^8 exosome particles were added to the co-culture corresponding to the TGF-β1 treatment with the exosome group. Five days after treatment, Masson's trichrome and immunocytochemistry were performed on the co-culture. For Masson's trichrome stain, cultures were treated overnight in Bouin's solution (Sigma). Slides were rinsed for 15 min under running water and stained with Weigert's haematoxylin (Sigma) for 10 min, after rinsed and stained with scarlet acid fuchsin (Sigma) for 5 min and rinsed again. Further, the slides were stained with phosphotunstic/phosphomolybdic acid (Sigma) for 3 min and aniline blue (Sigma) for 7 min and dried ethanol (50 and 100%) (Sigma) and xylenes for 1 min and mounted using DPX. For immunocytochemistry, cultures were fixed with 4% paraformaldehyde for 10 min, washed for 3 min with PBS followed by incubation with 0.1% Triton X-100 for 15 min, washed for 3 min with PBS, and blocked for 30 min (Protein block, serum-free), and overnight incubation with primary antibodies as follows: anti-vimentin antibody (1:500 abcam), anti-sarcomeric alpha actinin (1:800 abcam), Collagen I polyclonal antibody (1:500 Thermo Scientific). After overnight incubation, Alexa Fluor secondary antibodies were added as follows: anti-chicken Alexa Fluor 488 (1:600 Thermo Scientific), anti-mouse Alexa 594 (1:600 Thermo Scientific), and anti-rabbit Alexa 647 (1:600 Thermo Scientific), and mounted with fluroshield DAPI (Sigma Aldrich). The secondary antibody incubation time was 1 h followed by three PBS washes. Cells were imaged using confocal fluorescence microscope (Leica) at 20 μm.

Exosomes secreted by cardiosphere-derived cells sequencing

Nanostring

Cardiosphere-derived cell and fibroblast extracellular vesicles (EVs) were isolated from conditioned media using ultrafiltration (10 kDa molecular weight cut-off; Millipore). Total RNA was isolated from the filtrate using a miRNeasy mini-kit (Qiagen) per technical instructions. The input RNA quality was verified using Qubit miRNA assay (ThermoFisher). Analysis of miR counts was done using the Nanostring nCounter analysis system (Nanostring Technologies) with 15–150 ng of total RNA input from each sample. The set contained 800 probes derived from human miRBase version 3. Raw counts were obtained, normalized, and used for analysis. Values that fell below negative control levels were excluded from evaluation.

Next-generation sequencing

Total EV RNA was isolated from serum-free conditioned media of CDC EVs and normal human dermal fibroblast EVs was done using a silica-based EV capture followed by column RNA purification (Norgen Biotek). RNA was then sequenced using System Biosciences Inc.'s ExoNGS service which uses Illumina platform's NextSeq High Output single-end sequencing with NextSeq 500/550 High Output v2 kit (Illumina). Data processing was done using Maverix, Analytic Platform, and reads were curated for quality including filtering out including adaptor dimer sequences. Quality reads were enumerated, and sequences were aligned to reference genome (human) using Bowtie12 and only mappable reads were considered for evaluation.

Copy number curves

Concentrations (blank and 10^6–10^{11} copies) of miR-146a and miR-210 (GE Healthcare) mimics were used to generate a copy number curves. Extracellular vesicle RNA isolated a silica-based EV capture followed by column RNA purification (Norgen Biotek). To calculate the copy number per particle, EV concentration was measured in cleared conditioned media using nanosight tracking analysis using the following parameters: camera levels: 15; detection threshold: 5; videos taken per sample: 5; video duration: 60 s.

Statistical analysis

Data are presented as means ± standard deviation. The sample size was calculated based on pilot experiments that anticipated a 100% arrhythmia induction in controls, expecting a 20% reduction by CDC_{EXO} therapy. To achieve 80% power to detect such

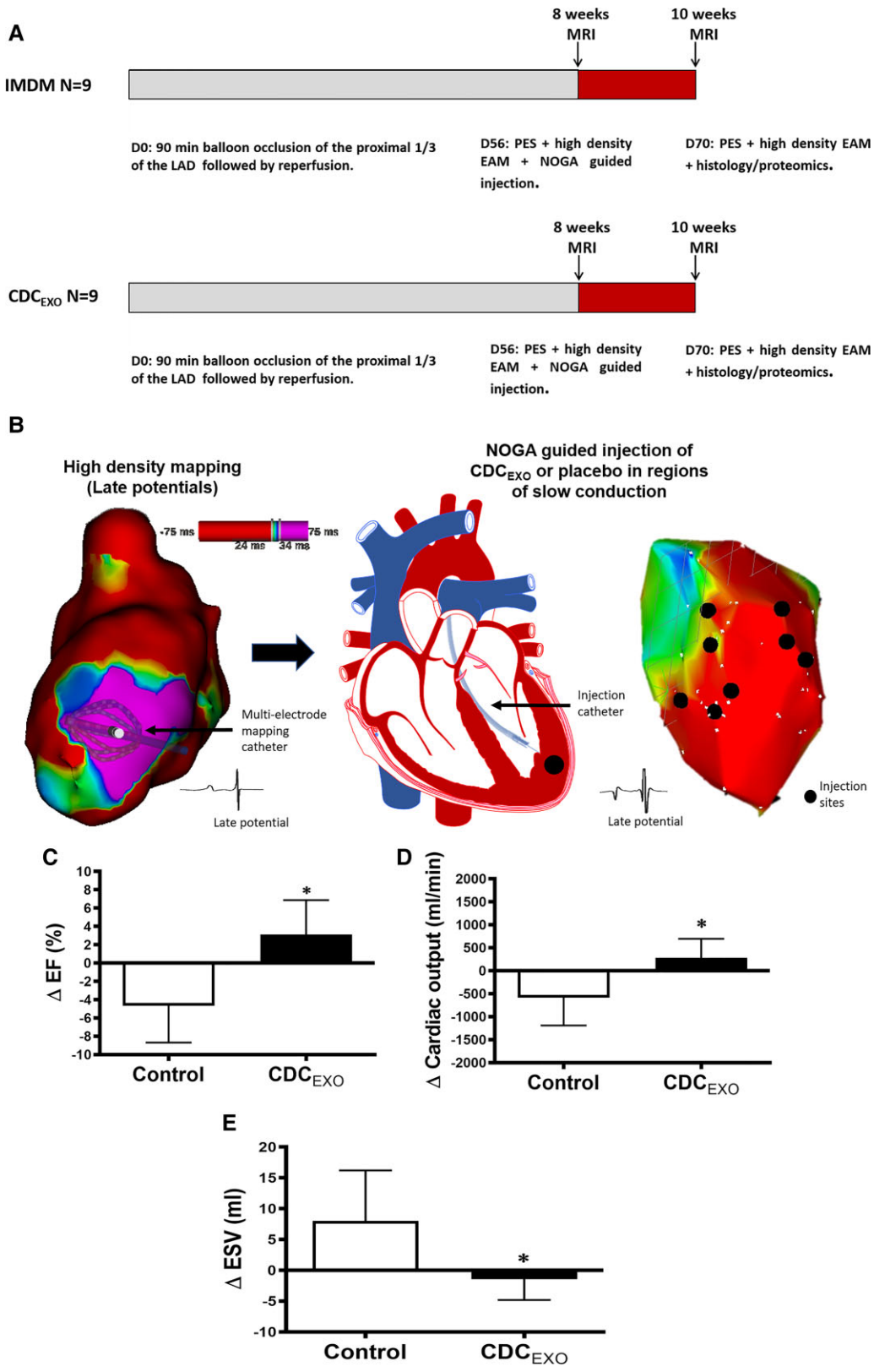

Figure 1 Experimental protocol and delivery technique. (*A*) Myocardial infarction was induced by 90 min balloon occlusion of the proximal anterior descending branch of the left coronary artery followed by 8 weeks of reperfusion. Cardiac function and scar size were examined by magnetic resonance imaging. Arrhythmia inducibility was probed by programmed electrical stimulation at the left ventricular scar border. If no sustained arrhythmia was induced, programmed electrical stimulation was repeated at the right ventricular apex. High-density

Continued

differences, a sample size of nine animals in each group was calculated. Power estimates were computed to be conservative assuming Fisher's exact test at the 0.013 alpha level to correct for multiple group comparisons. The primary endpoint (arrhythmia inducibility) was analysed using Fisher's exact test. Secondary outcomes of the scar size were analysed using repeated-measures analysis of variance of myocardial scar size over time within each treatment group followed by *post hoc* testing Bonferroni corrected for multiple comparisons. A two-tailed *t*-test was used to directly compare changes after intervention between CDC_{EXO} vs. control pigs.

Results

Arrhythmogenic substrate in swine model of ischaemic cardiomyopathy

Eight weeks post-MI, pigs were randomized to receive either CDC_{EXO} or vehicle (IMDM) and re-evaluated followed 2 weeks later (*Figure 1A*). After baseline MRI and PES, high-density activation mapping was performed to identify areas of slow conduction (assessed by the presence of ventricular late potentials)[3] during normal sinus rhythm. Areas of slow conduction were then verified using a NOGA® mapping system, and therapy was delivered using a NOGA®-compatible Myostar® catheter to those areas[20] (*Figure 1B*). Two weeks after treatment, follow-up phenotyping included MRI (to assess function and scar), high-definition EAM, and PES to assess arrhythmia inducibility. Afterwards, hearts were harvested for histology and proteomic analysis.

Structure and function of the left ventricle: improvement in left ventricular structure and function after exosomes secreted by cardiosphere-derived cells therapy

At the 2-week endpoint, MRI revealed improved systolic function with reduced chamber volumes in CDC_{EXO} pigs relative to controls. Left ventricular ejection fraction increased in CDC_{EXO} pigs but fell in control animals, together leading to a higher LVEF at endpoint in CDC_{EXO} pigs compared with vehicle (*Figure 1C* and see Supplementary material online, *Figure S1*). Likewise, the changes from baseline to endpoint in cardiac output (*Figure 1D*) revealed significant improvements in CDC_{EXO} pigs, but deterioration in controls. In addition to functional measures, dilatation of LV chamber volumes reflects the severity of cardiomyopathy. Left ventricular end-systolic volume was improved in CDC_{EXO} pigs but deteriorated in controls (*Figure 1E*), while increases in LV end-diastolic volume were attenuated in CDC_{EXO} pigs compared with controls (see Supplementary material online, *Figure S1* and Supplementary *Table S1*).

To determine if changes in global function and LV volumes were accompanied by reductions in scar burden, we used late gadolinium enhancement MRI. Our focal injection method was designed to diminish local scar in regions of slow conduction to modify the arrhythmogenic substrate. Thus, we utilized American Heart Association (AHA) segmented polar maps, and evaluated segments associated with the infarcted LAD territory (*Figure 2A*, *B* and *C*). Pooled data revealed decreases in scar size (%scar per LAD segment) in CDC_{EXO} pigs but not in controls (*Figure 2D*).

Electrophysiology study: decreased arrhythmia inducibility after exosomes secreted by cardiosphere-derived cells therapy

In 18 animals, PES was performed 8 weeks post-MI (baseline) and again 2 weeks after injection. At baseline, sustained VA could be induced in all animals randomized to the CDC_{EXO} group and in seven of nine control animals. In contrast, during the follow-up exam 2 weeks later, sustained arrhythmias were inducible in only two of nine CDC_{EXO} pigs, whereas VA were inducible in all control animals ($P = 0.015$; *Figure 3A*). Late potentials identified from high-density EAM (*Figure 3B*), indicative of slow conduction, were virtually eliminated in pigs receiving CDC_{EXO}, but persisted in control animals (*Figure 3C*). In addition, high-density EAM (*Figure 3E*) showed decreased areas of late activation on CDC_{EXO} pigs compared with controls (*Figure 3F* and *G*). Furthermore, isolated late potentials, previously identified within the arrhythmogenic substrate, were either completely absent or fused with the dominant electrogram signal to yield a multicomponent morphology at endpoint (*Figure 3D*). Conduction velocity throughout the arrhythmogenic substrate, determined by evaluating local activation times throughout the low-voltage scar area, was significantly increased in animals injected with CDC_{EXO}, directly corresponding with

Figure 1 Continued

three-dimensional electroanatomic mapping was then performed (Rhythmia®, Boston Scientific). Inducible animals were randomly assigned to receive focal injections of either 7.5 mg of CDC_{EXO} in 2 mL of IMDM or 2 mL of IMDM alone. Injections were performed in areas where late potentials were identified using electroanatomical mapping and confirmed by point-by-point mapping (NOGA®, Biosense Webster). Magnetic resonance imaging, electroanatomical mapping, and programmed electrical stimulation were repeated 2 weeks later. Animals were then euthanized, and the heart was removed for histologic and proteomic analysis. (*B*: Left) High-definition electroanatomical mapping image of the arrhythmogenic substrate with an identified late potential. (Centre) Schematic representation of delivery technique using intracardiac injection catheter (Myostar®, Biosense Webster). (Right) Representative NOGA® map with injection sites (black dots). (*C*) Animals injected with vehicle alone showed diminished contractile function (CDC_{EXO} 3.11 ± 3.75% vs. control −4.7 ± 4.04%, $P = 0.0006$). (*D*) Cardiac output increased in CDC_{EXO} pigs (CDC_{EXO} 278.1 ± 414 mL/min vs. control −586 ± 605 mL/min, $P = 0.0027$). (*E*) Deleterious changes in end-systolic volumes (CDC_{EXO} −1.4 ± 3.3 mL vs. control 8 ± 8.2 mL, $P = 0.005$) were observed in control but not in CDC_{EXO} pigs. A two-tailed *t*-test was used to compare the changes between groups.

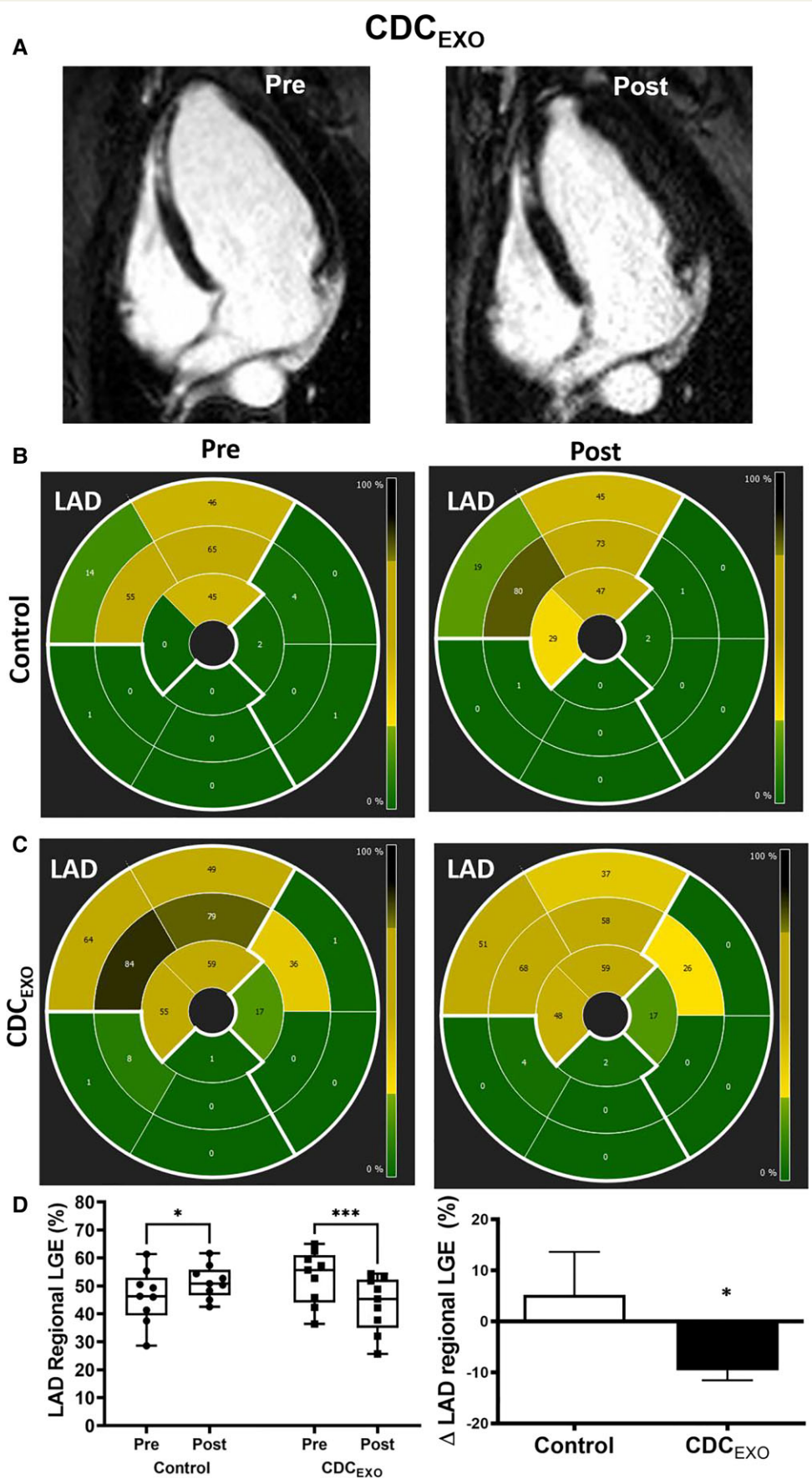

Figure 2 Myocardial scar by magnetic resonance imaging. (*A*) Representative four-chamber magnetic resonance image of infarcted ventricular myocardium identified by late gadolinium enhancement. Left is a baseline image pre-injection of CDC_{EXO} with follow-up examination 2 weeks

Continued

reductions in late diastolic potentials within the same area (*Figure 3H*).

Computational modelling of arrhythmogenesis: decreased re-entrant ventricular tachycardia *in silico* after exosomes secreted by cardiosphere-derived cells therapy

Anatomically based reconstructions of the infarcted human heart, coupled with experimentally constrained computational models of cardiac excitation, can reproduce clinically verified arrhythmogenesis.[9,21] Analysis of our experimental magnetic resonance images, performed independently by investigators blinded to group assignment, yielded reconstructed ventricular models (*Figure 4A*, top); however, the new analysis incorporated not only normal tissue and scar but also fuzzy regions (GZ) which correlate with arrhythmogenesis.[22] Following CDC_{EXO} injection, both scar and GZ in the inferior LV septal wall diminished (*Figure 4A*, bottom). Computational excitation of the reconstructed models, before CDC_{EXO} injection, revealed ready inducibility of sustained arrhythmias (*Figure 4B*, top) following pacing from the RV outflow tract; in contrast, after CDC_{EXO} treatment, VT was no longer inducible in the modelled heart (*Figure 4B*, bottom). The critical mechanism underlying sustained VT in the baseline LV was block of the anterior-septal wave travelling inferiorly (*Figure 4B*, bottom) at a region of endocardial scar, while other waves propagated undisturbed through the left and RV walls. These waves merged at the apex, managing to propagate superiorly through GZ tissue in the septal IZ and giving rise to sustained re-entry. In contrast, after CDC_{EXO}, the anterior-septal wave did not block because the amount of scar was decreased (*Figure 4B*, bottom). All propagating wavefronts then converged at the apex, resulting in conduction block and lack of sustained re-entry.

Histology: reduced fibrosis and increased cardiomyocyte proliferation after exosomes secreted by cardiosphere-derived cells therapy

Detailed examination of fibrosis by histology revealed less collagen within the IZ of CDC_{EXO} pigs compared with controls (*Figure 5A* and *B*). In the ischaemic zone of pigs injected with CDC_{EXO}, more actively dividing cardiomyocytes (double positive for α-SA and the mitotic marker Ki67) were evident than in controls (*Figure 5C* and *D*). This finding was confirmed by other markers of mitosis: there were significantly more phosphohistone H3+ cardiomyocytes (see Supplementary material online, *Figure S3*), and a trend for increased Aurora-kinase B+ cardiomyocytes, in the CDC_{EXO} group compared with controls (see Supplementary material online, *Figure S3*). Thus, CDC_{EXO} therapy not only attenuated fibrosis, but also promoted cardiomyocyte proliferation, consistent with previous findings.[23]

Proteomics: regulation of fibrosis, inflammation, and cell proliferation pathways by exosomes secreted by cardiosphere-derived cells therapy

For an unbiased evaluation of protein-level changes, we studied proteomics in six animals (three CDC_{EXO} vs. three control) to analyse samples of injected regions within the IZ, as well as samples from the BZ and RZ (i.e. non-infarcted) of the myocardium. Tissue was in-sequence digested,[24] and proteins were quantified by data-dependent acquisition MS analysed as described.[25] In total, 2329 unambiguously different proteins were identified by at least two unique peptides across all zones. Among these, 471 proteins showed differences ($P < 0.05$) between CDC_{EXO} and control animals across all zones (222 DEPs in the IZ, 106 DEPs in the BZ, and 187 DEPs in the RZ, with some, albeit few, changes being in common between tissue zones). Supplementary material online, *Table S3* lists DEPs for each zone with corresponding peptides in (see Supplementary material online, *Figure S4*). Within the IZ, CDC_{EXO}-injected tissue exhibited major pattern differences in pathways (see Supplementary material online, *Figure S4*) including those related to cell proliferation, inflammation, and fibrosis: the proteomic signatures were quite unique in CDC_{EXO} injected animals compared with controls (*Figure 5E* and *Table 1*). In fact, these protein changes are completely distinct from those identified in the BZ and RZ (*Figure 5E*, see Supplementary material online, *Figure S4*). The changes in pathways associated with fibrosis and the cell cycle underlie the histological findings of diminished scar and increased cardiomyocyte division in the same heart regions (*Figure 5A–D*). Among the specific protein changes, DHX9 (also known as RNA helicase A) was the most up-regulated in CDC_{EXO}-injected tissue (*Table 1*), with a >13-fold increase relative to controls. DHX9 is linked to multiple cellular functions including microRNA biogenesis, RNA processing and transport, maintenance of genomic stability,[26] and human fibroblast survival in culture.[27] Other proteins found to be increased greater than five-fold in CDC_{EXO} animals were STAT1 (a transcription factor involved in a variety of cell functions including the cell cycle and

Figure 2 Continued

later the right. (*B* and *C*) Representative polar maps with AHA segmentation highlighting the areas of enhancement in the anterior-septal regions of the heart perfused by the left anterior descending. The resolution of segmental colours from black to green reflects the reduction in scar per segment following focal delivery of IMDM, or IMDM + CDC_{EXO}. (*D*) Contrasting a modest increase in scar size in control animals, there was a reduction in scar size following focal injection of CDC_{EXO} at endpoint (CDC_{EXO} pre: 53.24 ± 3.21% vs. post: 43.40 ± 3.30%, $P = 0.0005$, control, pre: 46.24 ± 3.23% vs. post: 51.43 ± 1.07%, $P = 0.02$) (CDC_{EXO} −9.61 ± 1.92% vs. control: 5.18 ± 8.433%, $P = 0.0001$). Repeated-measures analysis of variance was used to analyse scar size pre and post. A two-tailed *t*-test was used for the statistical analysis of delta scar.

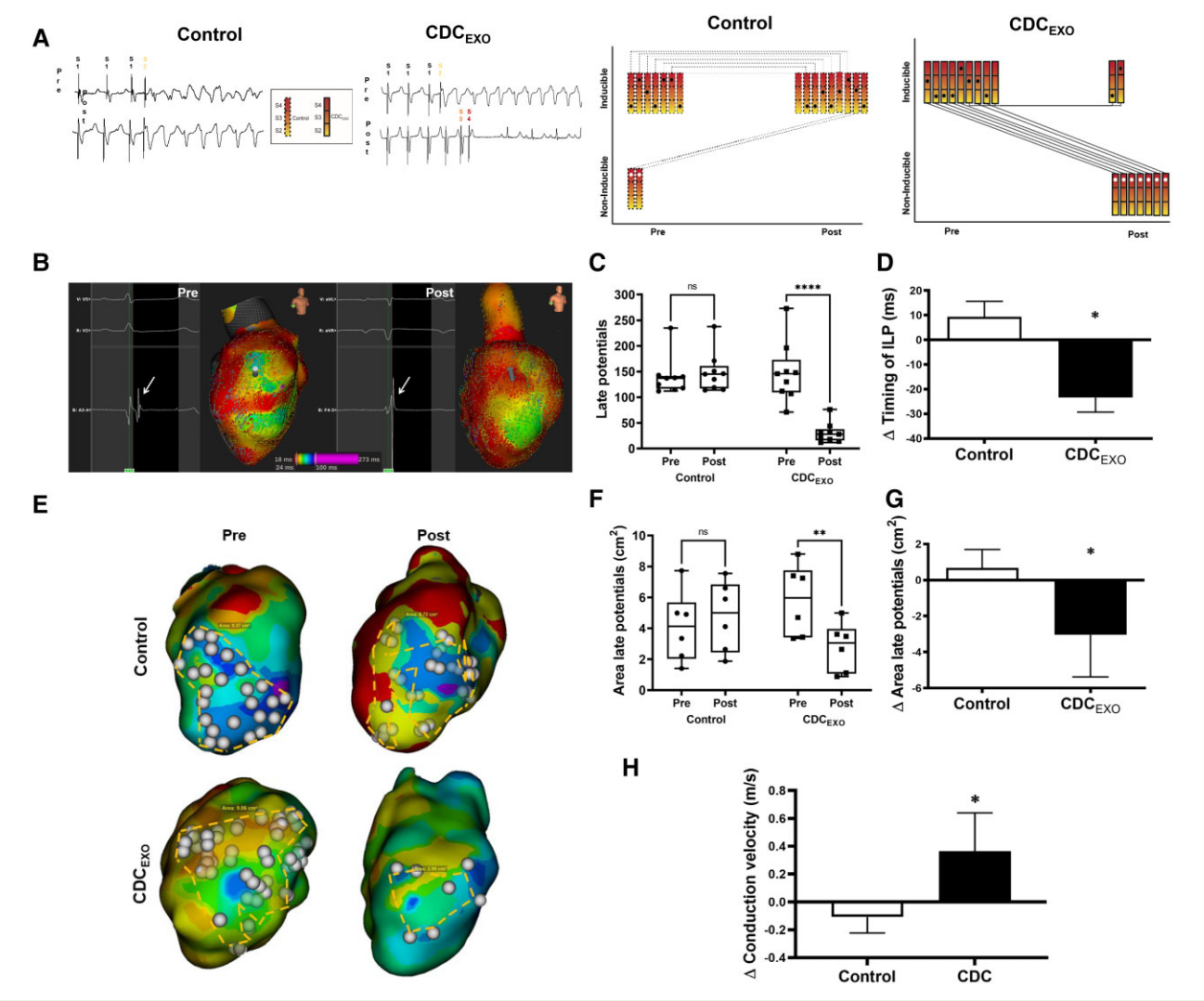

Figure 3 Ventricular arrhythmia inducibility and isolated late potentials. (*A*) Representative recordings of programmed electrical stimulation with corresponding extra stimuli in the same animal were performed 2 months after myocardial infarction, and repeated 2 weeks following injection with vehicle, control, or CDC_{EXO} (left). Programmed electrical stimulation was performed with as many as three extra stimuli with decreasing coupling intervals until the effective refractory period was reached from the left ventricular scar border zone and right ventricular apex. The colour scale reflects the degree of aggression in each animal pacing protocol by way of extra stimuli required to induce sustained VT, S2 being mild (yellow), and S4 being most aggressive (red). All inducible animals demonstrated sustained VT that was electrically cardioverted. Nine inducible pigs allocated to the CDC_{EXO} group displayed sustained ventricular arrhythmias at baseline; however, only two pigs remained inducible at endpoint, demonstrating an 80% reduction in sustained arrhythmias ($P = 0.015$ by Fisher's exact test). There was no reduction in arrhythmia inducibility in the pigs injected with vehicle only. Two of the control pigs were not inducible at baseline; however, all were inducible at endpoint (right). (*B*) Representative isolated late potential maps with corresponding electrograms from a CDC_{EXO} pig pre- and post-injection. The white arrows reflect the pre- and post-electrograms which reveal the disappearance of late potentials after CDC_{EXO} injection. (*C*) The amount of infarct associated late potentials was markedly reduced in animals injected with CDC_{EXO} (pre: 148.2 $\pm$ 58.3, post: 30.8 $\pm$ 19.8, $P < 0.0001$ by repeated-measures analysis of variance) but not in control (pre: 140.3 $\pm$ 37.3, post: 148.7 $\pm$ 38.6, $P =$ n.s. by repeated-measures analysis of variance). (*D*) Changes in timing of the late component of multicomponent intracardiac electrograms following injection of CDC_{EXO} or control (CDC_{EXO} −23.4 ms vs. control 9.3 ms, $P = 0.0004$ by two-tailed *t*-test). (*E*) Representative isochronal maps showing the reduction of areas of late activation in CDC_{EXO} pigs (*E*, bottom) when compared with controls (*E*, top). (*F*) CDC_{EXO} pigs demonstrated a far smaller area of late activation (pre: 5.82 $\pm$ 2.3 cm^2, post: 2.79 $\pm$ 1.57 cm^2, $P = 0.004$ by repeated-measures analysis of variance) when compared with controls (pre: 4.10 $\pm$ 2.27 cm^2, post: 4.778 $\pm$ 2.26 cm^2, $P =$ n.s. by repeated-measures analysis of variance). (*G*) Controls pigs showed an increased area of late potentials (0.67 $\pm$ 1.02 cm^2), in contrast with the decreased area seen in CDC_{EXO} pigs (−3.03 $\pm$ 2.35 cm^2) after therapy. $P = 0.005$ by two-tailed *t*-test. (*H*) Conduction velocity was calculated from Rhythmia activation maps and analysed with MATLAB. While there is a slowing in conduction velocity in control animals, conduction velocity is increased in CDC_{EXO}-treated pigs (−0.1082 $\pm$ 0.11 m/s, control; 0.361 $\pm$ 0.27, CDC_{EXO}, $P = 0.0005$ by two-tailed *t*-test).

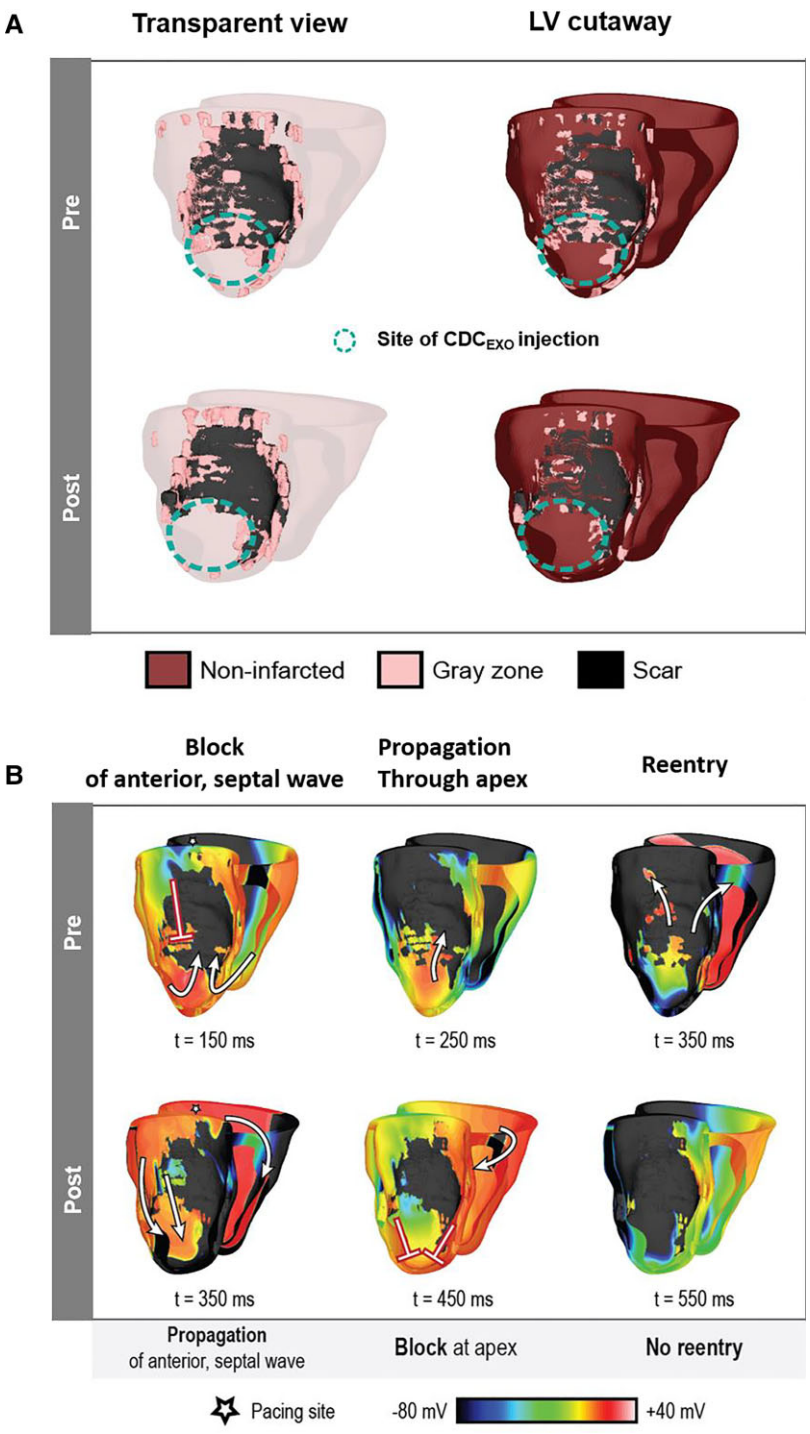

Figure 4 Anatomically based computational modelling of excitability. (*A*) Representative pre- (top) and post- (bottom) images of infarcted myocardium and associated grey zone before and after injection in a CDC_{EXO} animal, based on magnetic resonance imaging data. Note the overall decrease in scar and grey zone (volume fractions: scar: 16.57–12.69%; GZ: 7.22–6.93%). (*B*) Computational model of unilateral conduction block and associated re-entry circuit prior to injection with CDC_{EXO} (top). Afterwards, this potential re-entry channel is open and the wave-front conducts through the anterior myocardium and the apex in a more homogeneous fashion, without re-entry (bottom).

fibrosis), and desmoplakin (*Table 1*), a critical component of myocardial cell–cell signalling which has been linked to heritable arrhythmogenic cardiomyopathies.[28] While the proteomic changes only begin to hint at the underlying mechanisms of benefit, the findings are entirely in sync with extensive evidence that CDC_{EXO} not only promote cardiomyocyte proliferation, but also antagonize inflammation and fibrosis.[6] Such changes could synergistically decrease the arrhythmogenic substrate.

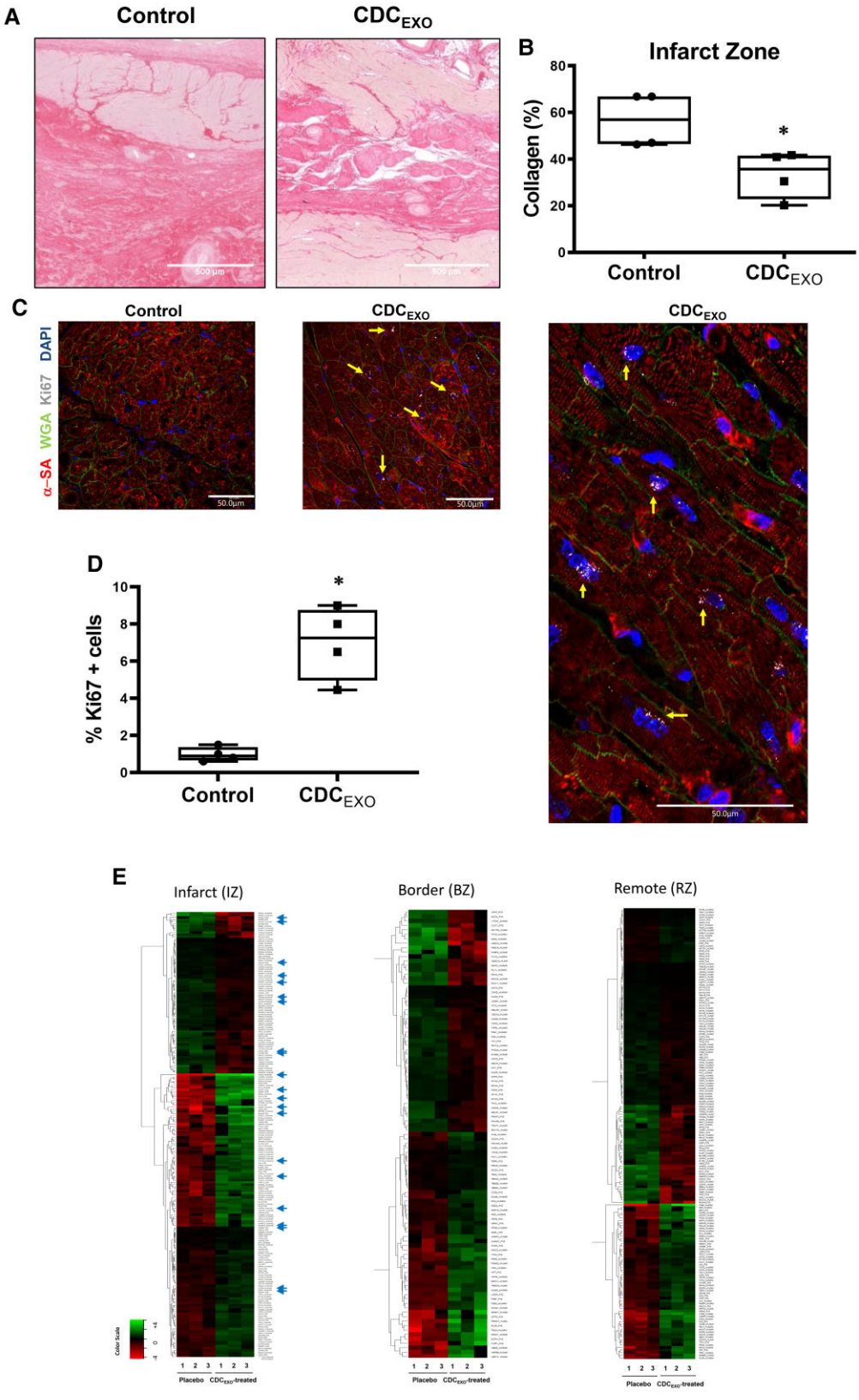

Figure 5 Fibrosis, cardiomyocyte proliferation, and proteomics. (*A*) Picrosirius red-stained sections of the infarct zone revealed reduced areas of fibrosis in the CDC_{EXO} pigs (CDC_{EXO} 33.3 ± 10.1%, $n = 4$ vs. control 56.7 ± 11.6%, $n = 4$, $P = 0.02$). (*B*) Ki67 immunostaining of viable tissue

Continued

In vitro fibrosis model: anti-fibrotic effects of exosomes secreted by cardiosphere-derived cells therapy

To further characterize the anti-fibrotic effects of CDC_{EXO}, we developed an *in vitro* cardiac fibrosis assay by mixing primary cardiac fibroblasts with ventricular cardiomyocytes in two-dimensional co-culture[29] (see Supplementary material online, *Figure S2A*). When TGF-β is added to stimulate the fibroblasts, the co-cultures develop interstitial fibrosis, evident either by collagen immunohistochemistry or by Masson's trichrome staining (see Supplementary material online, *Figure S2B–D*). On Day 5, each culture dish was randomly assigned to one of the three groups: control (vehicle), pirfenidone (a TGF-β inhibitor), or CDC_{EXO}. Immunohistochemistry revealed striking reductions in collagen by either CDC_{EXO} or pirfenidone (see Supplementary material online, *Figure S2B and C*). Similar effects were evident in representative Masson's trichome-stained images from each experimental group (see Supplementary material online, *Figure S2D*). These *in vitro* data support the notion that strong anti-fibrotic effects of CDC_{EXO} (comparable to those of the TGF-β inhibitor, pirfenidone) underlie the therapeutic benefits seen *in vivo*.

Longer follow-up group: decreased arrhythmogenic substrate by exosomes secreted by cardiosphere-derived cells 1 month post-injection

In classic substrate modification using radiofrequency ablation, efficacy is assessed acutely by testing VA inducibility. Given that our biological approach relies on slower, non-destructive mechanisms of action, we chose an initial 2-week follow-up for assessment of therapeutic efficacy. By this time, almost all animals were non-inducible by PES (*Figure 3*). To determine whether the benefits were durable, another cohort of 10 pigs was followed for a full month post-injection. Two of the 10 pigs died in the immediate MI setting due to VA, and one animal was excluded due to insufficient injury (global scar size $<5\%$ and LVEF $>55\%$) at baseline. Of the seven pigs evaluated at 1 month, four had been injected with CDC_{EXO} and three had received vehicle alone (*Figure 6A*). Regional scar size increased 1-month post-injection in the control animals, but quite the opposite was seen in the CDC_{EXO} pigs, where the changes in scar size were indicative of resolution of the substrate (*Figure 6B*, $P = 0.03$). Global function and structure were improved, as evidenced by an increase in LVEF in the CDC_{EXO} group (ΔEF, $P = 0.002$) and preservation of chamber volumes and cardiac output (*Figure 6C* and *D*). Programmed electrical stimulation showed no arrhythmia inducibility in any of the CDC_{EXO} pigs; however, sustained arrhythmias persisted in the control group. One control animal was neither inducible at baseline nor at endpoint. The considerable expense of chronic large animal studies precluded longer-term follow-up, but, at least for 1 month, the benefits of biological substrate modification persisted (*Figure 6F*).

Exosomes secreted by cardiosphere-derived cells characterization

Sequencing the RNA contents of CDC_{EXO} identified several miRs involved in fibrosis, immunomodulation, and regulation of pro-arrhythmic pathways (see Supplementary material online, *Figure S5A*). Absolute quantification of the selected miRs validates enrichment of these miRs (see Supplementary material online, *Figure S5B*). For instance, miR-27a targets early growth response protein (egr3), a potentiator of TGF-β signalling;[30] the miR attenuates cardiac fibrosis.[31] Similarly, miR-24 inhibits the TGF-β pathway through targeting furin and smad2. miR-22 attenuates cardiac remodelling and hypertrophy through its targets sirt1 and hdac4.[32] Perhaps most prominently, miR-146a and miR-210 have been shown by our group and others to regulate fibrosis and arrhythmia at multiple levels including myocyte death, inflammation, and fibrosis.[23,33,34] miR-210 regulates myocyte apoptosis and inflammation through targeting Ephrin A3 (EFNA3) and DR6, respectively.[35] Moreover, miR-146a is a master regulator of inflammation and fibrosis,[23,33,34] which has been implicated in regulating inflammation through modulation of neutrophil extracellular trap formation (netosis).[36] Quantitation against a standard curve confirms the abundance of these two key miRs in CDC_{EXO} (see Supplementary material online, *Figure S5C*).

Discussion

Conventional catheter ablation for VT seeks to interrupt critical areas of slow conduction within the circuits responsible for maintenance of the arrhythmia.[5] Most cardiomyopathy patients with VT exhibit haemodynamically unstable arrhythmias which cannot be

Figure 5 Continued

within the infarct zone of control and CDC_{EXO} pigs along with staining for identifiable proteins and structures within the mammalian cardiomyocyte at 20× (top) and 63× (bottom) (α-SA, alpha-sarcomeric actin; WGA, wheat germ agglutination; DAPI, 4′,6-diamidino-2-phenylindole). (*C* and *D*) More double positive Ki67+/α-SA+ cardiomyocytes were evident in CDC_{EXO} (yellow arrows) pigs while nearly undetectable in controls. At 63×, 1000 cardiomyocytes per animal were analysed yielding significantly more Ki67+/α-SA+ proliferating cardiomyocytes within the infarct zone of CDC_{EXO} pigs (CDC_{EXO} 6.98 ± 1.97% $n = 4$ vs. control 0.97 ± 0.38%, $n = 4$, $P = 0.001$). A two-tailed *t*-test was used for statistical analysis between groups (scale bar 50 μm). (*E*) The heat maps show mass spectrometry data fold changes (log2) of significantly changed proteins for the infarct zone, border zone, and remote zone identified in the human or pig database search. Fold changes between each analysed sample and the average of the compared treatment group [control 1, control 2, control 3 vs. average CDC_{EXO} ($n = 3$) and CDC_{EXO} 1, CDC_{EXO} 2, CDC_{EXO} 3 vs. average of control ($n = 3$)] were calculated from normalized MS2 spectral count data. The red colour indicates an increase in protein concentration relative to the compared treatment group and green a decrease, whereas the brightness of the colour represents the degree of fold change with brighter colours standing for and high fold change value and darker colours for a lower. The black colour indicates low fold change or missing data (protein failed to be identified). Blue arrows are proteins found.

Table 1 Most significant CDC_{EXO}-induced protein changes in the infarct zone

Protein name	Gene name-database species	Fold change (log2)	*P*-value	Protein accession number	Alternative protein names	Gene
ATP-dependent RNA helicase A	DHX9_HUMAN[a]	13.40	0.004	Q08211	DEAH box protein 9, Leucophysin, Nuclear DNA helicase II	DHX9
V-type proton ATPase subunit B	VATB2_HUMAN[b]	7.66	0.002	Q9Y6W5	V-ATPase subunit B 2, endomembrane proton pump 58 kDa subunit, HO57, vacuolar proton pump subunit B 2	ATP6V1B2
Tryptophan–tRNA ligase, cytoplasmic	SYWC_HUMAN[b]	6.47	0.041	Q9BQE3	Interferon-induced protein 53, IFP53, tryptophanyl-tRNA synthetase, TrpRS, hWRS	WARS
Vigilin	VIGLN_HUMAN[b]	6.10	0.018	P08670	HDL-binding protein	HDLBP
Septin-6	SEPT6_HUMAN[a]	5.88	0.009	Q07955		42984
Exportin-2	XPO2_HUMAN[a]	5.49	0.017	P55060	Cellular apoptosis susceptibility protein, chromosome segregation 1-like protein, importin-alpha re-exporter	CSE1L
Interleukin enhancer-binding factor 2	ILF2_HUMAN[a]	5.28	0.002	Q9UKU7	Nuclear factor of activated T-cells 45 kDa	ILF2
Desmoplakin	DESP_HUMAN[b]	5.27	0.001	Q9NR28	250/210 kDa paraneoplastic pemphigus antigen	DSP
Signal transducer and activator of transcription 1-alpha/beta	STAT1_PIG[c] *STAT1_HUMAN*	5.18	4 × E−5	Q764M5 *Q9UHP9*	Transcription factor ISGF-3 components p91/p84	STAT1
60 kDa SS-A/Ro ribonucleoprotein	RO60_HUMAN[a]	4.86	0.002	P10155	60 kDa Ro protein, 60 kDa ribonucleoprotein Ro, Ro 60 kDa autoantigen, Sjoegren syndrome antigen A2, joegren syndrome type A antigen, TROVE domain family member 2	TROVE2
RNA-binding protein 8A	RBM8A_HUMAN[a]	4.14	0.022	Q86TD4	Binder of OVCA1-1, BOV-1, RNA-binding motif protein 8A, RNA-binding protein Y14, ribonucleoprotein RBM8A	RBM8A
26S proteasome non-ATPase regulatory subunit 3	PSMD3_HUMAN[a]	3.62	0.035	O43242	26S proteasome regulatory subunit RPN3, 26S proteasome regulatory subunit S3, Proteasome subunit p58	PSMD3
Serine/arginine-rich splicing factor 1	SRSF1_ PIG[c] *SRSF1_HUMAN*	3.57	0.012	Q3YLA6 *Q13247*	Alternative-splicing factor 1, ASF-1, splicing factor, arginine/serine-rich 1, pre-mRNA-splicing factor SF2, P33 subunit	SRSF1
Coronin-1A	COR1A_HUMAN[b]	3.49	0.003	P31146	Coronin-like protein A, Clipin-A, coronin-like protein p57, tryptophan aspartate-containing coat protein, TACO	CORO1A
40S ribosomal protein S17	RS17_PIG[c] *RS17_HUMAN*	3.37	0.007	Q6QAP7 *P08708*	Small ribosomal subunit protein eS17	RPS17
Eukaryotic translation initiation factor 3 subunit J	EIF3J_HUMAN[a]	3.36	0.030	P06730	Eukaryotic translation initiation factor 3 subunit 1, eIF-3-alpha, eIF3 p35	EIF3J
Rho GTPase-activating protein 1	RHG01_HUMAN[b]	3.17	0.011	P62745	CDC42 GTPase-activating protein, GTPase-activating protein rhoGAP, Rho-related small GTPase protein activator, Rho-type GTPase-activating protein 1, p50-RhoGAP	ARHGAP1
TAR DNA-binding protein 43	TADBP_HUMAN[b]	3.11	0.046	P17987	TDP-43	TARDBP

All proteins identified are in the human annotated Uniprot database and in the databases described below.
[a]Protein in the pig unannotated Uniprot protein database.
[b]Protein not in either the pig annotated or unannotated Uniprot protein database.
[c]Present in the pig and human annotated Uniprot protein database and the amino acid sequence overlap between human, and pigs are 90% or higher (italicized is human information).

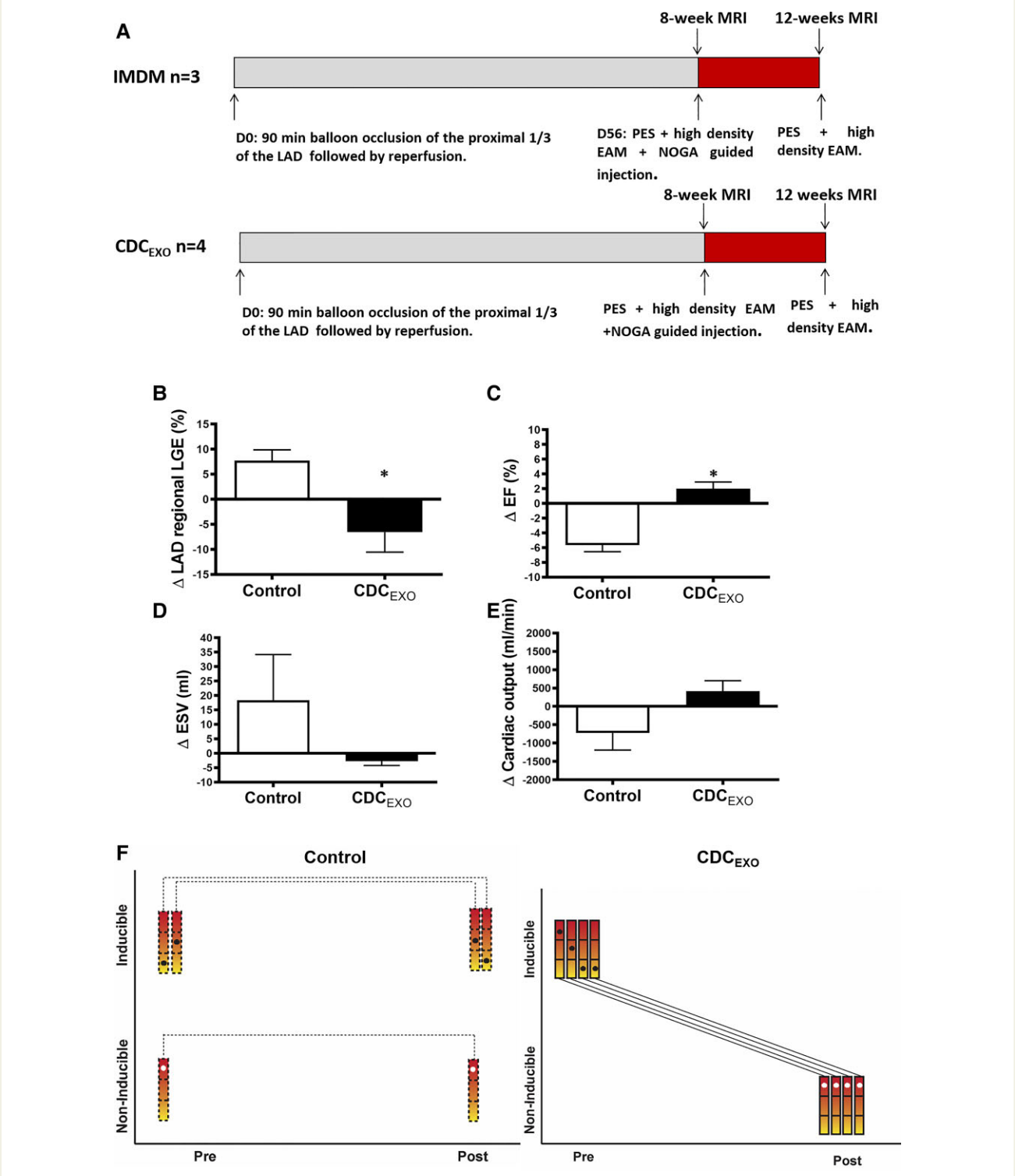

Figure 6 One-month follow-up study. (*A*) Experimental protocol similar to *Figure 1A*. To identify long-term therapeutic benefits, we followed the animals for an additional 4 weeks post-injection ($n = 3$ control, $n = 4$ CDC_{EXO}). (*B*) As observed in the short-term follow-up, there was a significant reduction in scar size around the area of injection perfused by the left anterior descending artery in CDC_{EXO} pigs (ΔCDC_{EXO} −6.55 ± 8% vs. control 7.723 ± 3.71%, $P = 0.03$). (*C*) Left ventricular function was preserved in CDC_{EXO} pigs (ΔCDC_{EXO} 2 ± 1.82% vs. control −5.66 ± 1.52%, $P = 0.002$) due to maintenance of chamber volume and cardiac output. (*D* and *E*) (ΔESV, CDC_{EXO} −2.75 ± 2.98 mL vs. control 18.33 ± 27.43 mL, $P =$ n.s., ΔCO, CDC_{EXO} 420 ± 561.89 mL/min vs. control −723.7 ± 804 mL/min, $P =$ n.s.). Changes between groups were analysed using two-tailed *t*-test. (*F*) Additionally, all the 1-month follow-up animals that received CDC_{EXO} were initially susceptible to inducible arrhythmias, became non-inducible, wherein the arrhythmogenic status of control animals remained the same at endpoint.

readily mapped,[37] leading to the strategy of substrate modification (also known as scar homogenization) by targeting late potentials.[38] Viable myocardium, identified by abnormal late electrograms, is targeted in a generalized manner, whether or not any given circuit can be shown to underlie the culprit arrhythmia.[39] Although substrate modification by catheter ablation is superior in outcomes to medical management alone,[40] such a 'carpet bombing' approach remains suboptimal. Recurrence rates are high; indeed, new areas of slow conduction and re-entry can develop from ablation lesions and related cardiac necrosis.[41] Here, we have implemented a non-destructive biological technique to diminish re-entry, based on the salutary effects of exosome therapy (notably including attenuation of fibrosis). Computational modelling of the arrhythmogenic substrate rationalized the experimental finding that re-entry was no longer sustained after exosome injection. Areas of conduction block, evident at baseline, were attenuated. Targeting areas of slow conduction by intramyocardial injection of CDC_{EXO} at the site of identifiable late potentials was effective to this end, as verified by a virtual disappearance of late potentials post-treatment; such potentials fused with the R wave to form a multi-component electrogram, which is less arrhythmogenic.[29,39] Most importantly, the therapeutic benefit of these changes was evidenced by lack of VA inducibility at a follow-up of either 2 weeks or 1 month.

The therapeutic paradigm tested here—injection of exosomes into zones of slow conduction—was designed to improve conduction by diminishing fibrosis in these areas. Indeed, within the region of injection, scar content was significantly decreased as quantified either by MRI (*Figure 2*) or by histology (*Figure 5*). Consistent with prior observations,[6,7] CDC_{EXO} were dramatically anti-fibrotic *in vitro* (Supplementary material online, *Figure S2*). The totality of the data supports the following mechanism of action: VT is rendered non-inducible by anti-fibrotic effects of CDC_{EXO}, which improve conduction in areas of isolated late potentials. By increasing tissue viability in areas of injection, the cardiomyogenic effects of CDC_{EXO} (evident in *Figure 5C* and *D* and see Supplementary material online, *Figure S3*) would, synergistically, potentiate the resolution of late potentials. The net result is CDC_{EXO} improve conduction and render the heart resistant to arrhythmia. *In silico* models of electrical conduction, empirically derived from cardiac magnetic resonance images, verified that the observed reductions in fibrosis sufficed to terminate re-entry in cases where CDC_{EXO} had been effective *in vivo*. Despite the intentionally local nature of the therapy, CDC_{EXO} injection improved global LV function (improved LVEF; *Figure 1C*) and structure (attenuated LV dilatation; *Figure 1E* and see Supplementary material online, *Figure S1*). The CDC_{EXO}-responsive myocardial proteome changes in the infarct zone are unique (different proteins and directionality) compared with those induced in the BZ and RZ, and include key pathways such as cell proliferation, inflammation, and fibrosis (*Figure 5E* and see Supplementary material online, *Figure S4*). Such global improvements may reflect enhanced cardiomyogenesis and/or greater co-ordination of contraction due to increased homogeneity of LV depolarization in the ischaemic zone with CDC_{EXO} treatment (*Figure 2B–E*). Regardless of the mechanism, the fact that LV function and structure are improved render biological substrate modification qualitatively different from ablation, in which tissue is destroyed and LV function is undermined.[42]

The findings of dramatic benefit should be tempered by recognition of limitations of the model, which is created by waiting 2 months post-MI before baseline phenotyping and therapeutic intervention. Although major inflammatory pathways associated with the acute ischaemic event had subsided by then, chronic remodelling mechanisms were still ongoing [as verified by the progressive LV dilatation seen in control animals (*Figure 1E*)]. In contrast, many ischaemic cardiomyopathy patients experiencing spontaneous arrhythmias have not suffered from recent MI. In patients with ischaemic cardiomyopathy, scar size serves as an independent predictor of sustained VA or ICD discharges.[43] Another limitation of our study lies in the fact that we have focused on biomarkers (late potentials, CV, PES inducibility, MRI parameters), rather than on ambient arrhythmias, to assess efficacy. Future studies will logically include telemetry to assess whether spontaneous episodes of VT are similarly suppressed. Linking a specific biologically active agent(s) present in the CDC_{EXO} to a specific proteomic pathway modulated in the ischaemic zone is of great interest, especially as several are predicted to be involved in cell proliferation, inflammation, and fibrosis have been identified (see Supplementary material online, *Figure S4*). This will be the focus of future studies. Finally, we have shown a reduction in VA inducibility 2 weeks post-injection (*Figure 3*), which persists up to 1-month post-injection (*Figure 6*); longer-term follow-up, while desirable, was beyond the scope of the present study.

Taken together, our findings support the anti-arrhythmic effects of CDC_{EXO} in a pre-clinical model of ischaemic cardiomyopathy. Focal delivery of CDC_{EXO} in areas of late activation represents a novel, non-destructive substrate modification strategy to prevent VT (*Graphical Abstract*). The biological product (CDC_{EXO}) can be readily manufactured to clinical standards and can be delivered using minimally invasive catheter technology which has been used extensively in clinical trials of other biological products (e.g. stem cells, angiogenic factors). Assessment of benefit in patients with recurrent VT would be straightforward, insofar as multiple surrogate biomarkers are available and well validated, and clinical event rates are high. Accordingly, biological substrate modification may merit clinical testing in patients with ischaemic cardiomyopathy and recurrent VA.

Limitations

Since there is no delivery catheter compatible with the high-density mapping system used (Rhythmia), we first performed a high-density map with a multi-electrode catheter (Orion/Rhythmia) to identify and quantify areas of late potentials. We then took fluoroscopic references using two orthogonal views and confirmed the existence of late potentials in those regions using a lower density map (point by point) with a NOGA system that was then utilized to deliver the EVs using a NOGA-guided Myostar injection catheter.

Supplementary material

Supplementary material is available at *European Heart Journal* online.

Acknowledgements

We would like to thank Catherine Bresee, MS, for help with statistical analysis. E.M. holds the Mark S. Siegel Family Foundation Distinguished Chair of the Cedars-Sinai Medical Center.

Funding

This study was funded by the National Institutes of Health (1K01HL133510-01A1 to J.F.D., R01 HL135866 to E.C. and E.M. and RO1 HL14750 to E.C.). N.T. is funded by the National Institutes of Health (DP1-HL123271 and R01HL116280), and a grant from the Leducq Foundation.

Conflict of interest: E.M. holds founder's equity in Capricor Inc. The other authors have no competing conflicts of interest to report.

Data availability

The authors declare that the data supporting the findings of this study are available within the paper. Raw data were generated at Cedars-Sinai Medical Center. Derived data supporting the findings of this study are available from the corresponding author upon request.

References

1. Ponikowski P, Voors AA, Anker SD, Bueno H, Cleland JGF, Coats AJS, *et al.* ESC guidelines for the diagnosis and treatment of acute and chronic heart failure: the Task Force for the diagnosis and treatment of acute and chronic heart failure of the European Society of Cardiology (ESC) developed with the special contribution of the Heart Failure Association (HFA) of the ESC. *Eur Heart J* 2016;**37**:2129–2200.
2. Poole JE, Johnson GW, Hellkamp AS, Anderson J, Callans DJ, Raitt MH, *et al.* Prognostic importance of defibrillator shocks in patients with heart failure. *N Engl J Med* 2008;**359**:1009–1017.
3. Anter E, Tschabrunn CM, Buxton AE, Josephson ME. High-resolution mapping of postinfarction reentrant ventricular tachycardia electrophysiological characterization of the circuit. *Circulation* 2016;**134**:314–327.
4. Sapp JL, Wells GA, Parkash R, Stevenson WG, Blier L, Sarrazin JF, *et al.* Ventricular tachycardia ablation versus escalation of antiarrhythmic drugs. *N Engl J Med* 2016;**375**:111–121.
5. Aliot EM, Stevenson WG, Almendral-Garrote JM, Bogun F, Calkins CH, Delacretaz E, *et al.* EHRA/HRS Expert Consensus on Catheter Ablation of Ventricular Arrhythmias: developed in a partnership with the European Heart Rhythm Association (EHRA), a Registered Branch of the European Society of Cardiology (ESC), and the Heart Rhythm Society (HRS); in collaboration with the American College of Cardiology (ACC) and the American Heart Association (AHA). *Heart Rhythm* 2009;**6**:886–933.
6. Marban E. A mechanistic roadmap for the clinical application of cardiac cell therapies. *Nat Biomed Eng* 2018;**2**:353–361.
7. Gallet R, Dawkins J, Valle J, Simsolo E, de Couto G, Middleton R, *et al.* Exosomes secreted by cardiosphere-derived cells reduce scarring, attenuate adverse remodelling, and improve function in acute and chronic porcine myocardial infarction. *Eur Heart J* 2017;**38**:201–211.
8. Cassidy DM, Vasallo JA, Miller JM, Poll DS, Buxton AE, Marchlinski FE, *et al.* Endocardial catheter mapping in patients in sinus rhythm: relationship to underlying heart disease and ventricular arrhythmias. *Circulation* 1986;**73**:645–652.
9. Prakosa A, Malamas P, Zhang S, Pashakhanloo F, Arevalo H, Herzka DA, *et al.* Methodology for image-based reconstruction of ventricular geometry for patient-specific modeling of cardiac electrophysiology. *Prog Biophys Mol Biol* 2014;**115**:226–234.
10. Deng D, Arevalo H, Pashakhanloo F, Prakosa A, Ashikaga H, McVeigh E, *et al.* Accuracy of prediction of infarct-related arrhythmic circuits from image-based models reconstructed from low and high resolution MRI. *Front Physiol* 2015;**6**:282.
11. Bayer JD, Blake RC, Plank G, Trayanova NA. A novel rule-based algorithm for assigning myocardial fiber orientation to computational heart models. *Ann Biomed Eng* 2012;**40**:2243–2254.
12. Arevalo HJ, Vadakkumpadan F, Guallar E, Jebb A, Malamas P, Wu KC, *et al.* Arrhythmia risk stratification of patients after myocardial infarction using personalized heart models. *Nat Commun* 2016;**7**:11437.
13. Rodriguez B, Li L, Eason JC, Efimov IR, Trayanova NA. Differences between left and right ventricular chamber geometry affect cardiac vulnerability to electric shocks. *Circ Res* 2005;**97**:168–175.
14. Herrington DM, Mao C, Parker SJ, Fu Z, Yu GQ, Chen L, *et al.* Proteomic architecture of human coronary and aortic atherosclerosis. *Circulation* 2018;**137**:2741–2756.
15. Golden HB, Gollapudi D, Gerilechaogetu F, Li J, Cristales RJ, Peng X, *et al.* Isolation of cardiac myocytes and fibroblasts from neonatal rat pups. *Methods Mol Biol* 2012;**843**:205–214.
16. Middleton RC, Rogers RG, De Couto G, Tseliou E, Luther K, Holewinski R, *et al.* Newt cells secrete extracellular vesicles with therapeutic bioactivity in mammalian cardiomyocytes. *J Extracell Vesicles* 2018;**7**:1456888.
17. de Couto G, Jaghatspanyan E, DeBerge M, Liu W, Luther K, Wang Y, *et al.* Mechanism of enhanced MerTK-dependent macrophage efferocytosis by extracellular vesicles. *Arterioscler Thromb Vasc Biol* 2019;**39**:2082–2096.
18. Kapoor N, Liang W, Marbán E, Cho HC. Direct conversion of quiescent cardiomyocytes to pacemaker cells by expression of Tbx18. *Nat Biotechnol* 2013;**31**:54–62.
19. Mastikhina O, Moon BU, Williams K, Hatkar R, Gustafson D, Mourad O, *et al.* Human cardiac fibrosis-on-a-chip model recapitulates disease hallmarks and can serve as a platform for drug testing. *Biomaterials* 2020;**233**:119741.
20. Yee K, Malliaras K, Kanazawa H, Tseliou E, Cheng K, Luthringer DJ, *et al.* Allogeneic cardiospheres delivered via percutaneous transendocardial injection increase viable myocardium, decrease scar size, and attenuate cardiac dilatation in porcine ischemic cardiomyopathy. *PLoS One* 2014;**9**:e113805.
21. Trayanova NA, Pashakhanloo F, Wu KC, Halperin HR. Imaging-based simulations for predicting sudden death and guiding ventricular tachycardia ablation. *Circ Arrhythm Electrophysiol* 2017;**10**:e004743.
22. Schmidt A, Azevedo CF, Cheng A, Gupta SN, Bluemke DA, Foo TK, *et al.* Infarct tissue heterogeneity by magnetic resonance imaging identifies enhanced cardiac arrhythmia susceptibility in patients with left ventricular dysfunction. *Circulation* 2007;**115**:2006–2014.
23. Hirai K, Ousaka D, Fukushima Y, Kondo M, Eitoku T, Shigemitsu Y, *et al.* Cardiosphere-derived exosomal microRNAs for myocardial repair in pediatric dilated cardiomyopathy. *Sci Transl Med* 2020;**12**:eabb3336.
24. Kane LA, Neverova I, Van Eyk JE. Subfractionation of heart tissue: the 'in sequence' myofilament protein extraction of myocardial tissue. *Methods Mol Biol* 2007;**357**:87–90.
25. Andres AM, Kooren JA, Parker SJ, Tucker KC, Ravindran N, Ito BR, *et al.* Discordant signaling and autophagy response to fasting in hearts of obese mice: implications for ischemia tolerance. *Am J Physiol Heart Circ Physiol* 2016;**311**:H219–H228.
26. Karin M, Anning L. NF-kappaB at the crossroads of life and death. *Nat Immunol* 2002;**3**:221–227.
27. Lee T, Di Paola D, Malina A, Mills JR, Kreps A, Grosse F, *et al.* Suppression of the DHX9 helicase induces premature senescence in human diploid fibroblasts in a p53-dependent manner. *J Biol Chem* 2014;**289**:22798–22814.
28. Castelletti S, Vischer AS, Syrris P, Crotti L, Spazzolini C, Ghidoni A, *et al.* Desmoplakin missense and non-missense mutations in arrhythmogenic right ventricular cardiomyopathy: genotype-phenotype correlation. *Int J Cardiol* 2017;**249**:268–273.
29. Hsia HH, Lin D, Sauer WH, Callans DJ, Marchlinski FE. Relationship of late potentials to the ventricular tachycardia circuit defined by entrainment. *J Interv Card Electrophysiol* 2009;**26**:21–29.
30. Fang F, Shangguan AJ, Kelly K, Wei J, Gruner K, Ye B, *et al.* Early growth response 3 (Egr-3) is induced by transforming growth factor-beta and regulates fibrogenic responses. *Am J Pathol* 2013;**183**:1197–1208.
31. Teng L, Huang Y, Guo J, Li B, Lin J, Ma L, *et al.* Cardiac fibroblast miR-27a may function as an endogenous anti-fibrotic by negatively regulating Early Growth Response Protein 3 (EGR3). *J Cell Mol Med* 2021;**25**:73–83.
32. Huang ZP, Chen J, Seok HY, Zhang Z, Kataoka M, Hu X, *et al.* MicroRNA-22 regulates cardiac hypertrophy and remodeling in response to stress. *Circ Res* 2013;**112**:1234–1243.
33. Ibrahim AG, Cheng K, Marban E. Exosomes as critical agents of cardiac regeneration triggered by cell therapy. *Stem Cell Reports* 2014;**2**:606–619.
34. Barile L, Lionetti V, Cervio E, Matteucci M, Gherghiceanu M, Popescu LM, *et al.* Extracellular vesicles from human cardiac progenitor cells inhibit cardiomyocyte apoptosis and improve cardiac function after myocardial infarction. *Cardiovasc Res* 2014;**103**:530–541.
35. Zhang D, Cao X, Li J, Zhao G. MiR-210 inhibits NF-kappaB signaling pathway by targeting DR6 in osteoarthritis. *Sci Rep* 2015;**5**:12775.
36. Arroyo AB, de Los Reyes-Garcia AM, Rivera-Caravaca JM, Valledor P, Garcia-Barbera N, Roldan V, *et al.* MiR-146a regulates neutrophil extracellular trap formation that predicts adverse cardiovascular events in patients with atrial fibrillation. *Arterioscler Thromb Vasc Biol* 2018;**38**:892–902.
37. Santangeli P, Marchlinski FE. Substrate mapping for unstable ventricular tachycardia. *Heart Rhythm* 2016;**13**:569–583.

38. Kumar S, Baldinger SH, Romero J, Fujii A, Mahida SN, Tedrow UB, *et al.* Substrate-based ablation versus ablation guided by activation and entrainment mapping for ventricular tachycardia: a systematic review and meta-analysis. *J Cardiovasc Electrophysiol* 2016;**27**:1437–1447.
39. Bogun F, Good E, Reich S, Elmouchi D, Igic P, Lemola K, *et al.* Isolated potentials during sinus rhythm and pace-mapping within scars as guides for ablation of post-infarction ventricular tachycardia. *J Am Coll Cardiol* 2006;**47**:2013–2019.
40. Reddy VY, Reynolds MR, Neuzil P, Richardson AW, Taborsky M, Jongnarangsin K, *et al.* Prophylactic catheter ablation for the prevention of defibrillator therapy. *N Engl J Med* 2007;**357**:2657–2665.
41. Yokoyama K, Nakagawa H, Wittkampf FH, Pitha JV, Lazzara R, Jackman WM. Comparison of electrode cooling between internal and open irrigation in radiofrequency ablation lesion depth and incidence of thrombus and steam pop. *Circulation* 2006;**113**:11–19.
42. Siontis KC, Kim HM, Vergara P, Peretto G, Do DH, de Riva M, *et al.* Arrhythmia exacerbation after post-infarction ventricular tachycardia ablation: prevalence and prognostic significance. *Europace* 2020;**22**:1680–1687.
43. Klem I, Weinsaft JW, Bahnson TD, Hegland D, Kim HW, Hayes B, *et al.* Assessment of myocardial scarring improves risk stratification in patients evaluated for cardiac defibrillator implantation. *J Am Coll Cardiol* 2012;**60**:408–420.